Organic & Biomolecular Chemistry

PAPER

View Article Online
View Journal | View Issue

Check for updates

Cite this: *Org. Biomol. Chem.*, 2017, **15**, 5719

Exploiting the biosynthetic machinery of *Streptomyces pilosus* to engineer a water-soluble zirconium(IV) chelator†

Tomas Richardson-Sanchez, ‡ William Tieu, ‡ Michael P. Gotsbacher, Thomas J. Telfer and Rachel Codd *

The water solubility of a natural product-inspired octadentate hydroxamic acid chelator designed to coordinate Zr(IV)-89 has been improved by using a combined microbiological-chemical approach to engineer four ether oxygen atoms into the main-chain region of a methylene-containing analogue. First, an analogue of the trimeric hydroxamic acid desferrioxamine B (DFOB) that contained three main-chain ether oxygen atoms (DFOB-O_3) was generated from cultures of the native DFOB-producer *Streptomyces pilosus* supplemented with oxybis(ethanamine) (OBEA), which competed against the native 1,5-diaminopentane (DP) substrate during DFOB assembly. This precursor-directed biosynthesis (PDB) approach generated a suite of DFOB analogues containing one (DFOB-O_1), two (DFOB-O_2) or three (DFOB-O_3) ether oxygen atoms, with the latter produced as the major species. Log *P* measurements showed DFOB-O_3 was about 45 times more water soluble than DFOB. Second, a peptide coupling chain-extension reaction between DFOB-O_3 and the synthetic ether-containing *endo*-hydroxamic acid monomer 4-((2-(2-aminoethoxy)ethyl)(hydroxy)amino)-4-oxobutanoic acid (PBH-O_1) gave the water soluble tetrameric hydroxamic acid DFOB-O_3–PBH-O_1 as an isostere of sparingly water soluble DFOB–PBH. The complex between DFOB-O_3–PBH-O_1 and ^{nat}Zr(IV), examined as a surrogate measure of the radiolabelling procedure, analysed by LC-MS as the protonated adduct ($[M + H]^+$, m/z_{obs} = 855.2; m/z_{calc} = 855.3), with supporting HRMS data. The use of a microbiological system to generate a water-soluble analogue of a natural product for downstream semi-synthetic chemistry is an attractive pathway for developing new drugs and imaging agents. The improved water solubility of DFOB-O_3–PBH-O_1 could facilitate the synthesis and purification of downstream products, as part of the ongoing development of ligands optimised for Zr(IV)-89 immunological PET imaging.

Received 4th May 2017,
Accepted 20th June 2017

DOI: 10.1039/c7ob01079f

rsc.li/obc

Published on 20 June 2017. Downloaded by University of Sydney on 2/26/2024 10:29:47 PM.

Introduction

Evaluating the potential of emerging radiometals for use in nuclear medicine requires ligands designed to bind the radiometal with high affinity and high selectivity.[1–4] Zirconium(IV)-89 is one radiometal gathering traction for use in immunological positron emission tomography (PET) imaging, due to two complementary properties.[5–12] First, its relatively low positron emission energy (23%, β+ 0.396 MeV) gives images with intrinsic spatial resolution similar to F-18, and better than higher energy β+ radionuclides. Second, its 3.27-day half-life is matched with the circulation half-life of antibodies. This allows a Zr(IV)-89-antibody complex to selectively accumulate over 2–4 days at the tumor to increase radiotracer uptake and imaging sensitivity, compared to radionuclides with shorter half-lives. Multiple preclinical[13–17] and clinical[18–22] studies have shown the promise of immunological Zr-89 PET imaging, which has prompted studies on the design of bifunctional ligands that selectively coordinate Zr(IV)-89 and contain a covalently bound peptide or antibody. The ligand commonly used for this purpose is the hydroxamic acid-based siderophore desferrioxamine B (DFOB) (Fig. 1, **1**),[5,6,23] which is a secondary metabolite produced by *Streptomyces pilosus* and other actinomycetes to sequester local Fe(III) for bacterial iron supply.[24–26] The hydroxamic acid functional groups of DFOB are well suited to coordinate the hard acid Zr(IV) and the term-

School of Medical Sciences (Pharmacology) and Bosch Institute, The University of Sydney, New South Wales 2006, Australia. E-mail: rachel.codd@sydney.edu.au; Tel: +61 2 9351 6738

†Electronic supplementary information (ESI) available: Additional data for the ether-containing DFOB analogues (LC-MS, MS/MS, NMR spectroscopy, HRMS), PBH-O_1, the chain-extension products DFOB-O_3-PBH-O_1 and DFOB-PBH-O_1 (NMR spectroscopy, HRMS), and ^{nat}Zr(IV)-DFOB-O_3-PBH-O_1 (HRMS). See DOI: 10.1039/c7ob01079f

‡These authors contributed equally to this work.

Published on 20 June 2017. Downloaded by University of Sydney on 2/26/2024 10:29:47 PM.

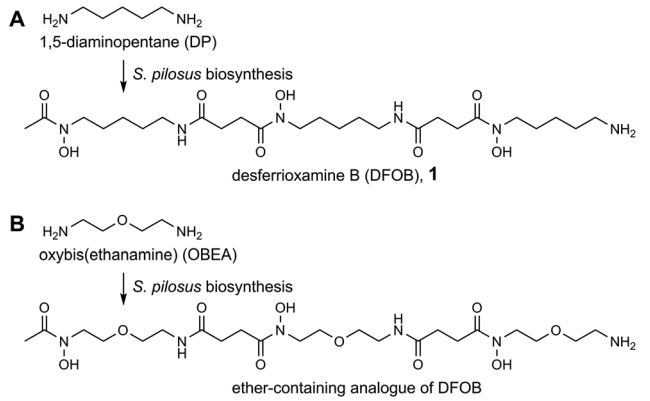

Fig. 1 Biosynthesis of (A) desferrioxamine B (DFOB, 1) from the native substrate 1,5-diaminopentane (DP) or (B) an ether-containing analogue of DFOB from the non-native substrate oxybis(ethanamine) (OBEA).

inal amine group allows the conjugation of biomolecules. Hexadentate DFOB, however, has been evolved to saturate the octahedral Fe(III) coordination sphere, and is unable to saturate the preferred octadentate coordination sphere of Zr(IV).[27,28] This can result in the Zr-89 radiolabel leaching from the complex to reduce image quality, and based on animal studies, the potential for deposition of the radiolabel in bone.[14,29–32] The suboptimal performance of hexadentate DFOB identified the need to generate octadentate ligands with improved selectivity for Zr-89.[27,33–35] An advance in Zr(IV) ligand design was provided with the chain-extension reaction between DFOB and 4-((5-aminopentyl)(hydroxy)amino)-4-oxobutanoic acid (PBH) to form DFOB–PBH that contained the requisite four bidentate hydroxamic acid functional groups and a preserved amine terminus.[34] Octadentate DFOB–PBH retained Zr(IV) more strongly than hexadentate DFOB, which supported the design principle of extending the DFOB scaffold by chain-extension. Unaware of this work in progress at the time, our group was undertaking the same chemistry and prepared DFOB–PBH as a Zr(IV) selective ligand. What was unexpected by us, and by the authors of the first-published[34] and more recent literature,[36] was the sparing water solubility of DFOB–PBH, which led to difficulties in purifying DFOB–PBH and its even more insoluble derivatives required for biomolecule conjugation. The sparing water solubility of DFOB–PBH was surprising, since DFOB itself is very water soluble ($\log P$ −2.10).[37] This led us to consider producing a second-generation analogue of DFOB–PBH with increased water solubility. The ideal pathway was one that made minimal changes to DFOB–PBH, since aside from water solubility, its properties as a ligand for immunological Zr-89 PET imaging were ideal.

This work conceived that a simple exchange of one or more methylene groups for ether oxygen atom(s) in the main-chain region of DFOB could produce ether-containing DFOB analogues as the start scaffold in the chain-extension reaction. The ether-containing DFOB analogues were predicted to be more water soluble than DFOB, which could improve the water solubility of downstream semi-synthetic constructs. This approach would incur a minimal increase in molecular weight, compared to more conventional strategies used to improve water solubility, such as PEGylation.[38,39]

Precursor-directed biosynthesis (PDB) was identified as a streamlined path with the potential to produce ether-containing DFOB analogues, with this method used previously to produce ether-containing macrocyclic hydroxamic acids.[40,41] PDB relies on the biosynthetic machinery of a native organism accepting non-native substrates during metabolite assembly[42] and is attractive in circumventing multistep chemical synthesis, as necessary for DFOB.[43] The biosynthesis of DFOB is well understood,[26,44,45] with assembly dependent upon 1,5-diaminopentane (DP) as the major endogenous diamine substrate, as produced from the decarboxylation of L-lysine (Fig. 1A). Unsaturated analogues of linear DFOB have been produced using PDB from bacterial culture medium supplemented with unsaturated non-native diamine substrates that compete with native DP.[26]

In this work, the ether-containing diamine substrate oxybis(ethanamine) (OBEA) was examined as a non-native substrate with potential to compete against native DP in DFOB assembly to produce new analogues of DFOB with improved water solubility (Fig. 1B). These water-soluble DFOB analogues could be used as scaffolds in chain-extension reactions to produce a new class of Zr-89 selective ligand with improved water solubility. This work describes the success in meeting this goal and highlights the value of PDB for re-engineering natural products to meet clinical needs.

Results and discussion

Supplementation of *S. pilosus* culture medium with OBEA

Cultures of *S. pilosus* were supplemented with OBEA at 5 mM, 10 mM or 20 mM to determine optimal levels of siderophore production and to establish any OBEA toxicity. The cultures grew well under OBEA supplementation at each concentration, and compared to the control showed increased siderophore production, as determined using an Fe(III) addition assay (Fig. 2). This demonstrated that OBEA was not toxic to *S. pilosus* and that the levels of exogenous diamine substrate in addition to the endogenous DP substrate enhanced siderophore biosynthesis. Balancing the cost of the OBEA substrate against increased siderophore production led to the selection of the mid-range concentration of 10 mM OBEA for ongoing experiments.

Precursor-directed biosynthesis of ether-containing analogues of DFOB

Culture supernatants were harvested at 8 days after OBEA supplementation and purified using a two-step procedure involving XAD-2 resin, and Ni(II)-IMAC resin, which is an affinity-based method used to purify hydroxamic acid siderophores from complex mixtures.[25,46–48] The semi-purified samples were analysed by liquid chromatography-mass spectrometry (LC-MS) to identify the number and relative concentration of

 This journal is © The Royal Society of Chemistry 2017

Published on 20 June 2017. Downloaded by University of Sydney on 2/26/2024 10:29:47 PM.

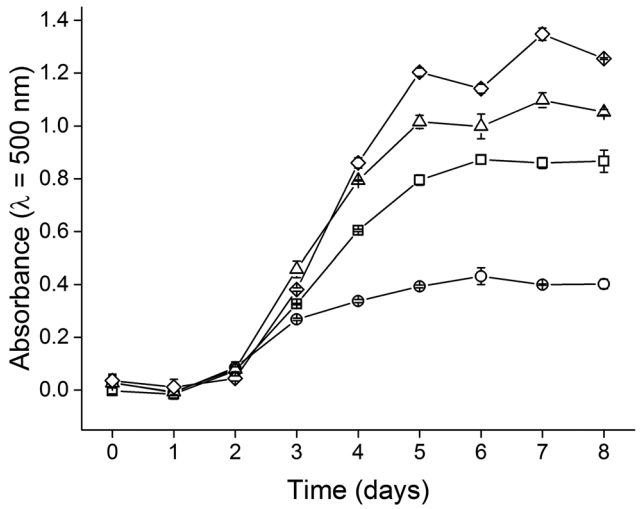

Fig. 2 Siderophore production (average of 3 measurements from Fe(III) addition assay) over 8 days in cultures of *S. pilosus* without supplementation (circle) or supplemented with OBEA at 5 mM (square), 10 mM (triangle) or 20 mM (diamond).

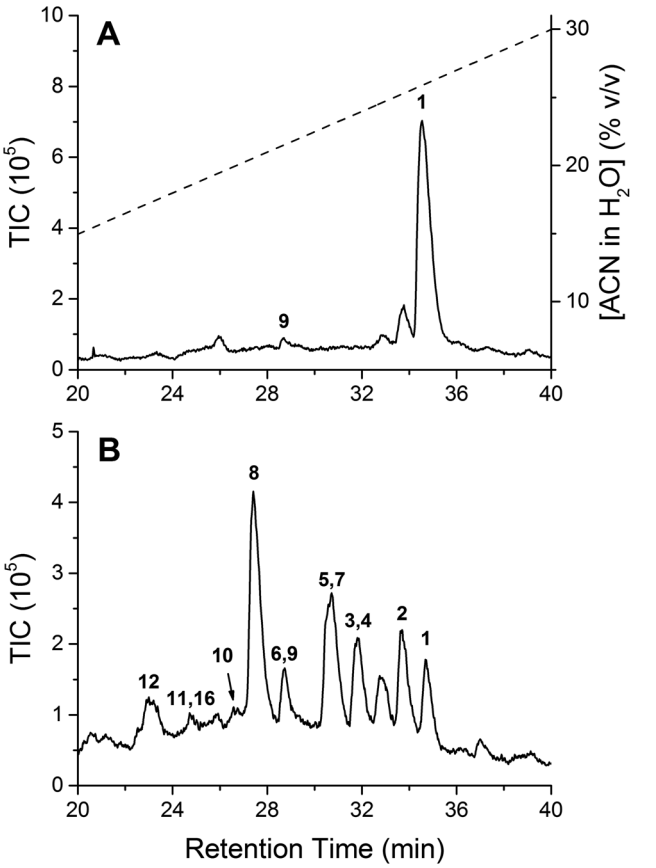

Fig. 3 LC-MS trace (TIC detection) from the semi-purified supernatant of *S. pilosus* cultured in medium containing no supplement (**A**) or supplemented with 10 mM OBEA (**B**). Peak labels refer to the compounds in Fig. 4. The gradient in (**A**) was the same in (**B**) and has been omitted for clarity.

siderophores. The control cultures of *S. pilosus* were processed and analysed in the same way.

The LC-MS trace from the control culture (Fig. 3A) showed a major signal at t_R 34.69 min that analysed as the protonated adduct of DFOB (m/z_{obs} = 561.3). The less intense signal at t_R 33.77 min corresponded with $DFOA_1$ (m/z_{obs} = 547.3), which is a native siderophore assembled from two DP substrates and one 1,4-diaminobutane substrate, which is produced as an endogenous substrate in low levels from the decarboxylation of L-ornithine.[24–26,48,49] The LC-MS trace from the OBEA-supplemented culture showed multiple, well resolved signals. In addition to a signal representing DFOB (t_R 34.69 min), which was significantly reduced in intensity compared to the native system, there were six new signals that eluted between t_R 27.42–33.70 min (Fig. 3B). The LC signal at t_R = 33.70 min gave an MS signal (m/z_{obs} = 563.4) consistent with a DFOB analogue that contained one ether oxygen atom, arising from the replacement of one native DP substrate with one non-native OBEA substrate (see ESI, Fig. S1†).

DFOB can be deconstructed into three unique regions, defined as the region containing the *N*-acetyl terminus, the internal region, and the region containing the amine terminus. The incorporation of non-native substrates into DFOB analogues gives rise to the possibility of the formation of constitutional isomers. Recent convention has used a binary nomenclature system to identify these isomers, where 0 = native substrate, 1 = non-native substrate; with the position in the trimer coded from left-to-right, as corresponding to the *N*-acetyl region, the internal region, and the amine region.[26] In the case of the DFOB analogues that contain one DP-for-OBEA substrate exchange, the three constitutional isomers are: DFOB-O_1[001] (**2**), DFOB-O_1[010] (**3**) and DFOB-O_1[100] (**4**) (Fig. 4). Each isomer can be identified from a signature MS/MS fragmentation pattern.[26] MS/MS fragmentation analysis (Fig. S2, Table S1†) identified the signal at t_R = 33.70 min as DFOB-O_1[001] (**2**). The signals for DFOB-O_1[010] (**3**) and DFOB-O_1[100] (**4**) co-eluted at t_R = 31.81 min. A second set of constitutional isomers (m/z_{obs} = 565.3) can be formulated for DFOB analogues that contain two DP-for-OBEA substrate exchanges: DFOB-O_2[011] (**5**), DFOB-O_2[110] (**6**) and DFOB-O_2[101] (**7**). The signal for DFOB-O_2[011] (**5**) and DFOB-O_2[101] (**7**) co-eluted at t_R = 30.72 min. The signal for DFOB-O_2[110] (**6**) at t_R = 28.74 min co-eluted with a non-ether-containing dimeric precursor (**9**) of native DFOB, which was also present in the native system. The complete DP-for-OBEA substrate exchange gave DFOB-O_3[111] (**8**) as a unique compound (m/z_{obs} = 567.3) eluting at t_R 27.42 min, which was produced as the siderophore in highest relative concentration. This was consistent with previous results that showed the DFOE analogue containing three DP-for-OBEA substrate exchanges was preferentially formed above analogues containing one or two OBEA-derived units.[40] The ether-containing DFOB analogues retained metal coordinating function, as determined from LC-MS data acquired from a solution with added Fe(III) (Fig. S1†).

Published on 20 June 2017. Downloaded by University of Sydney on 2/26/2024 10:29:47 PM.

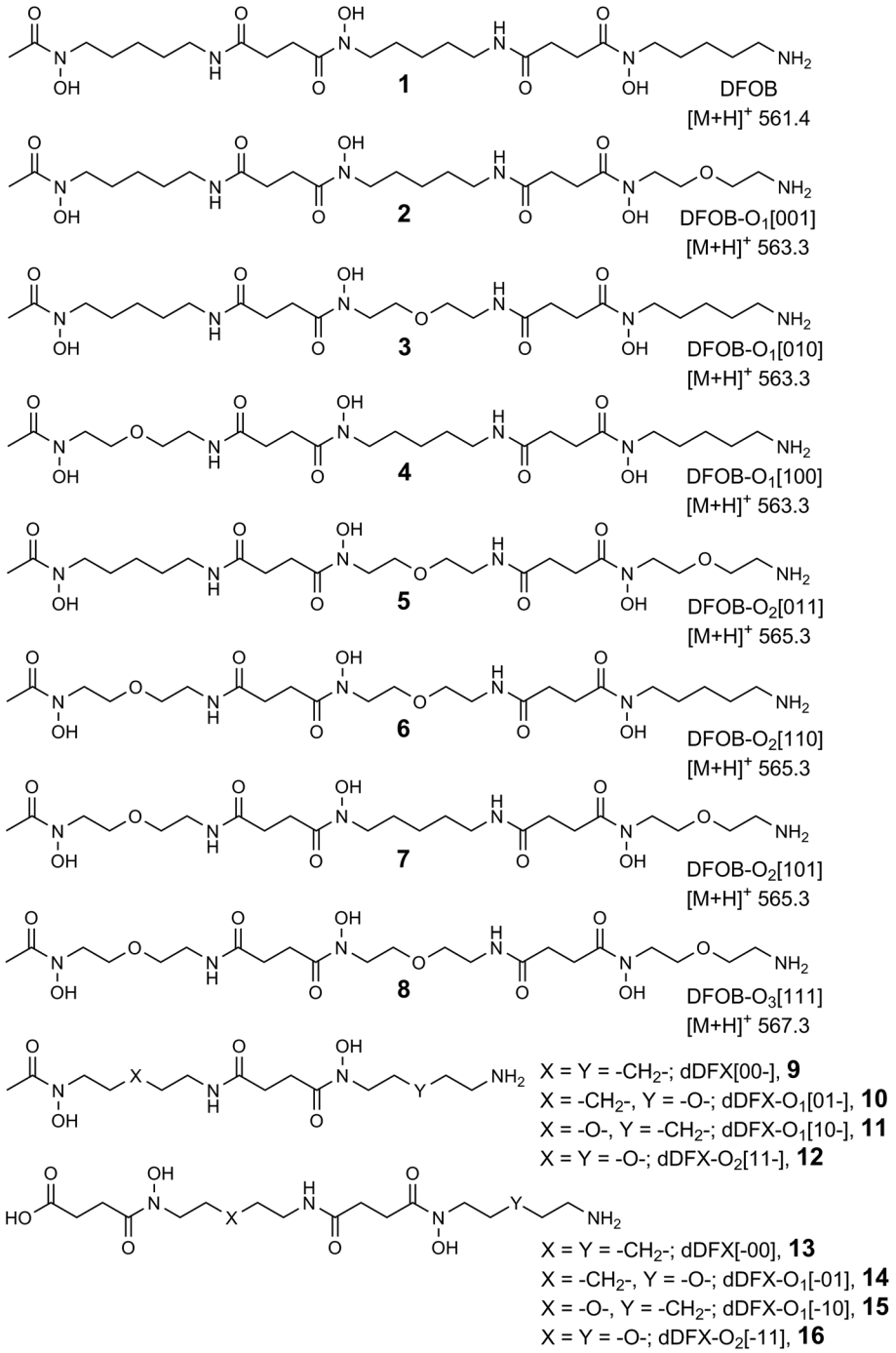

Fig. 4 DFOB (**1**) and analogues (**2–8**) assembled by *S. pilosus* in medium supplemented with OBEA, containing one (**2–4**), two (**5–7**) or three (**8**) ether oxygen atoms, with MS values ($[M + H]^+$, calculated). Selected dimeric compounds (**9–16**) were also postulated from MS and MS/MS data.

Trimeric DFOB is assembled from dimeric precursors, which can be detected *in situ*. Signals ascribable to the dimeric precursors as assembled in the direction from the *N*-acetylated region: dDFX[00-] (where 'd' indicates 'dimer' and '-' indicates the vacant position) (**9**), dDFX-O_1[01-] (**10**), dDFX-O_1[10-] (**11**) and dDFX-O_2[11-] (**12**) were present between t_R 23.09–28.74 min. Of the other set of dimeric precursors as assembled in the direction from the amine terminus, only dDFX[-11] (**16**) was observed experimentally (t_R 25.54 min). The relative concentration of the trimeric (**2–8**) and postulated dimeric (**9–16**) species, including the distribution of the constitutional isomers within the set of DFOB-O_1 and DFOB-O_2 series, was consistent with the distribution of unsaturated DFOB analogues and dimeric precursors that were produced using a PDB approach in a previous study.[26]

 This journal is © The Royal Society of Chemistry 2017

Published on 20 June 2017. Downloaded by University of Sydney on 2/26/2024 10:29:47 PM.

The relative concentrations of **1–8** showed that the DP-for-OBEA substrate exchange in DFOB assembly occurred in an overall ratio of 1 : 2.4, which compared well with the DP : OBEA incorporation ratio of 1 : 4 in the production of DFOE analogues.[40] The DP : OBEA incorporation ratio in the current work was 8 times greater than the incorporation of the butane-based substrate 1,4-diamino-2(*E*)-butene,[26] which could be attributed to the closer structural similarity of the pentane-based OBEA to DP.

Water solubility of ether-containing analogues of DFOB

Generating DFOB analogues that contained ether oxygen atoms in the main-chain region was undertaken to confer additional water solubility on constructs that could be used as reagents for downstream semi-synthetic chemistry. The insertion of one, two or three ether oxygen atoms into the DFOB analogues correlated with a systematic reduction in the RP-HPLC retention time, as an indirect measure of the increased solvation. Log *P* values were determined using the shake-flask method as a direct measure of water solubility for analogues that were sufficiently resolved to enable isolation using semi-preparative HPLC. The yields of compounds isolated by semi-preparative HPLC from one 50 mL culture broadly reflected the relative concentrations of the isomers in the supernatant: DFOB-O_1[001] (**2**) (1.2 mg), DFOB-O_2[110] (**6**) (2.2 mg) and DFOB-O_3[111] (**8**) (8.6 mg). These compounds were the best resolved from the mixture and furnished one isomer from each group (DFOB-O_1, DFOB-O_2, DFOB-O_3). The experimental log *P* values of DFOB-O_1[001] (**2**), DFOB-O_2[110] (**6**) and DFOB-O_3[111] (**8**) were in reasonable agreement with the calculated values (Table 1, Fig. S3†). Each of DFOB-O_1[001] (**2**), DFOB-O_2[110] (**6**) and DFOB-O_3[111] (**8**) were characterised by ^{1}H NMR spectroscopy (Fig. S4–S7†) and HRMS (Table S2†). DFOB-O_3[111] (**8**) was characterised by ^{13}C NMR spectroscopy (Fig. S8†).

Relative to DFOB, DFOB-O_1[001] (**2**), DFOB-O_2[110] (**6**) or DFOB-O_3[111] (**8**) were about 2.2, 43 or 45 times more water soluble. This showed benefit in engineering the exchange of methylene group(s) for ether oxygen atom(s) to increase the water solubility of a natural product. The marked increase in water solubility of DFOB-O_2[110] (**6**) or DFOB-O_3[111] (**8**) incurred only a modest increase in molecular weight (Fig. 5) and circumvented a potential undesirable increase in the molecular weight of DFOB that would arise from a more conventional water solubilising strategy such as PEGylation. Grafting onto DFOB a tri- or tetraethyleneglycol unit, for example, would result in an increase in molecular weight of 27 or 35%, respectively. Within each set of constitutional isomers, compounds with the OBEA substrate inserted at the *N*-acetylated region eluted earlier on the RP-HPLC system, which reflected some potential differences in the inherent water solubility and/or the nature of the interaction with the matrix of the C18 stationary phase.

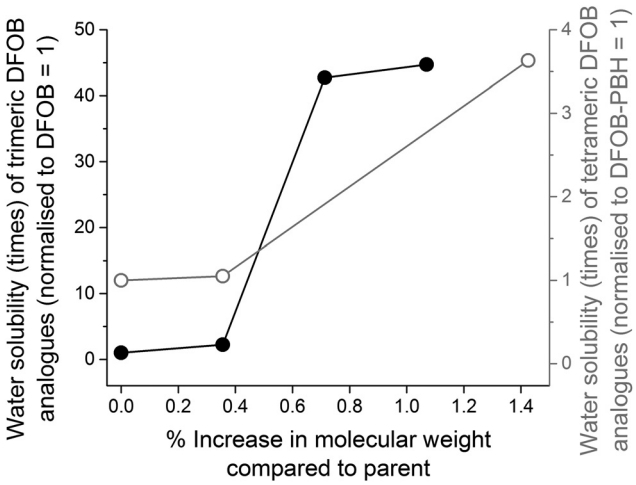

Fig. 5 Relative water solubility of trimeric ether-containing DFOB analogues normalised to DFOB (solid circle) or of tetrameric ether-containing DFOB analogues normalised to DFOB–PBH (open circle), *versus* % increase in molecular weight of the parent.

^{1}H and ^{13}C NMR spectroscopy of DFOB and DFOB-O_3[111]

The purity of DFOB-O_3[111] (**8**) allowed for a more extensive analysis by NMR spectroscopy, compared to DFOB-O_1[001] (**2**) and DFOB-O_2[110] (**6**), which were <90% pure. The three internal methylene groups of the three DP-based units of DFOB (positions 5–7, 16–18 and 27–29 (refer Table S4† for atom labelling)) gave signals in the ^{1}H or ^{13}C NMR spectra at δ_H 1.2–1.5 ppm or δ_C 23–29 ppm, respectively, in agreement with data derived from DP and literature.[50,51] The ^{1}H and ^{13}C chemical shifts for the methylene groups positioned alpha to the ether oxygen

Table 1 LC-MS data and log *P* values of DFOB and DFOB–PBH, and ether-containing analogues

No.	Name	$[M + H]^+_{calc}$	$[M + H]^+_{obs}$	t_R [a] (min)	t_R [b] (min)	log P_{exp} [c]	log P_{calc} [d]	H_2O sol.[e]
1	DFOB	561.4	561.4	34.69	18.87	−2.22	−2.75	1.0[f]
2	DFOB-O_1[001]	563.3	563.4	33.70	ND[h]	−2.57	−3.49	2.24[f]
6	DFOB-O_2[110]	565.3	565.3	28.74	ND	−3.85	−3.94	42.7[f]
8	DFOB-O_3[111]	567.3	567.3	27.42	16.49	−3.87	−4.67	44.7[f]
17	DFOB–PBH	761.5	761.4	ND	21.22	−2.35	−3.77	1.0[g]
18	DFOB–PBH-O_1	763.5	763.4	ND	20.42	−2.37	−4.51	1.05[g]
19	DFOB-O_3–PBH-O_1	769.4	769.3	ND	17.63	−2.91	−6.28	3.63[g]

[a] Gradient of 0–30% ACN : H_2O (40 min at 0.2 mL min^{-1}). [b] Gradient of 0–50% ACN : H_2O (45 min at 0.5 mL min^{-1}). [c] Determined from shake-flask method (average of duplicate measurements). [d] Determined using Advanced Chemistry Development Software V12.0. [e] Normalised water solubility (experimental). [f] Normalised to **1**. [g] Normalised to **17**. [h] ND = not determined.

Published on 20 June 2017. Downloaded by University of Sydney on 2/26/2024 10:29:47 PM.

atom in OBEA were δ_H 3.63 ppm and δ_C 66.3 ppm, respectively. The incorporation of internal ether oxygen atoms in DFOB-O_3[111] (**8**) (positions 6, 17 and 28) resulted in a downfield shift in the signals for the adjacent methylene groups. The absence of signals in the ^{1}H NMR spectrum of DFOB-O_3[111] (**8**) at δ_H 1.2–1.5 and the presence of signals at δ_H 3.1–3.6 ppm, was consistent with the proposed structure. HSQC analysis revealed correlations of protons at δ_H 3.39 and 3.53 ppm with carbon atoms at δ_C 68.3 and 65.9 ppm, respectively (Fig. 6). The triplet multiplicity and coupling constants (J = 5.9 and 5.5 Hz) of these signals were consistent with the incorporation of the OBEA units. Comprehensive NMR spectroscopic characterisation of DFOB-O_3[111] (**8**) as the major PBD-generated product is presented in the ESI (Table S4, Fig. S9–S11†).

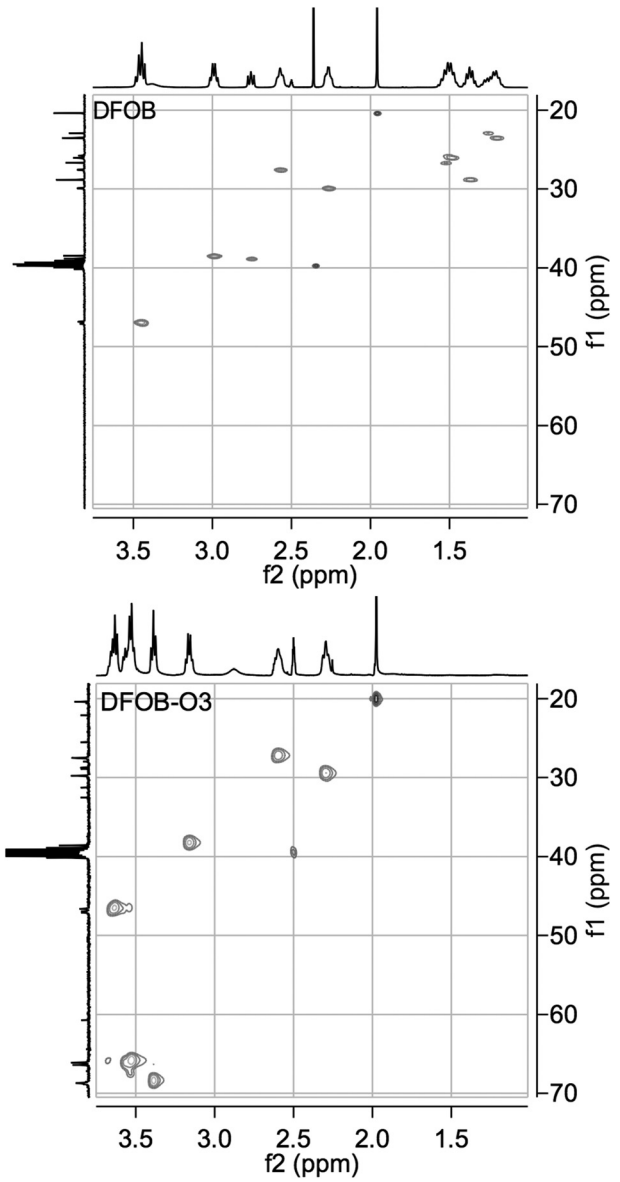

Fig. 6 Expansions of ^{1}H–^{13}C HSQC NMR spectra (400 MHz, DMSO-d_6) for DFOB (**1**) (upper) and DFOB-O_3 (**8**) (lower).

Chain-extension reaction using DFOB-O_3[111]

As found by others[34,36] and as developed in parallel in our laboratory, the peptide coupling reaction between DFOB and PBH gave the chain-extended product DFOB–PBH (**17**), which was close to insoluble in water. The design of DFOB–PBH was otherwise well optimised to form a stable 1 : 1 octadentate complex with Zr(IV), that retained the terminal amine amenable for biomolecule conjugation. The potential to improve water solubility of this type of construct was examined from a chain-extension reaction between DFOB and 4-((2-(2-aminoethoxy)ethyl)(hydroxy)amino)-4-oxobutanoic acid (PBH-O_1) to produce mono-ether-containing DFOB–PBH-O_1 (**18**) or between DFOB-O_3 and PBH-O_1 to produce tetra-ether-containing DFOB-O_3–PBH-O_1 (**19**) (Fig. 7). As hydrogen-bond acceptors, the ether groups were predicted to improve water solubility, but as weak donor atoms, not to compete against the hydroxamic acid groups for Zr(IV) coordination.

The ether-containing *endo*-hydroxamic acid monomer PBH-O_1 was prepared using methods adapted from the literature,[10,34] starting from 1,1′-oxybis[2-bromoethane] (Scheme S1†), with standard peptide coupling conditions used to prepared the tetrameric constructs (Fig. S12–S14†). Unlike the linear trimers (**1**, **2**, **6**, **8**), there were significant differences in the experimental and calculated log *P* values for the linear tetramers (**17**–**19**), with the compounds predicted to be much more water soluble than was found experimentally (Table 1). This could be due to the extended length of the tetramer and/or the presence of an additional amide bond in the chain-extended product inducing some secondary structure that attenuated solvation. The algorithm for the calculated log *P* values would not account for these structural subtleties. Other studies of DFOB-amide conjugates as new iron chelating compounds have observed significant differences in water solubility, with solvation properties dependent on the nature and steric bulk of the ancillary group, and likely modulated by secondary structure.[37,52] Ultimately, there appears to be an attenuation in water solubility upon conjugating any entity to DFOB, including an *endo*-hydroxamic acid monomer. Although the increase in water solubility of DFOB-O_3–PBH-O_1 (**19**) was modest (3.6 times) compared to DFOB–PBH (**17**) (Fig. 5), the principal goal of conferring additional water solubility upon a linear tetrameric hydroxamic acid was met. In practical terms, it was possible to obtain an ^{1}H NMR spectrum of **19** in D_2O at a concentration of 4 mg mL^{-1}, which was not possible for **17**. The increased water solubility of **19** above **17** could improve the ease of synthesis and purification of derivatives, as required for downstream biomolecule conjugation. The trend in the reversed-phase HPLC retention times of the series of tetrameric DFOB analogues (earlier to later: **19** < **18** < **17**) was in accord with the increasing order of water solubility (Fig. 8).

Complexation between DFOB-O_3–PBH-O_1 (19) and ^{nat}Zr(IV)

The complexation between DFOB-O_3–PBH-O_1 (**19**) and ^{nat}Zr(IV) was examined as a surrogate of the radiolabelling procedure. The LC-MS trace from a solution of ^{nat}Zr(acac)$_4$ (5 : 1

 This journal is © The Royal Society of Chemistry 2017

Published on 20 June 2017. Downloaded by University of Sydney on 2/26/2024 10:29:47 PM.

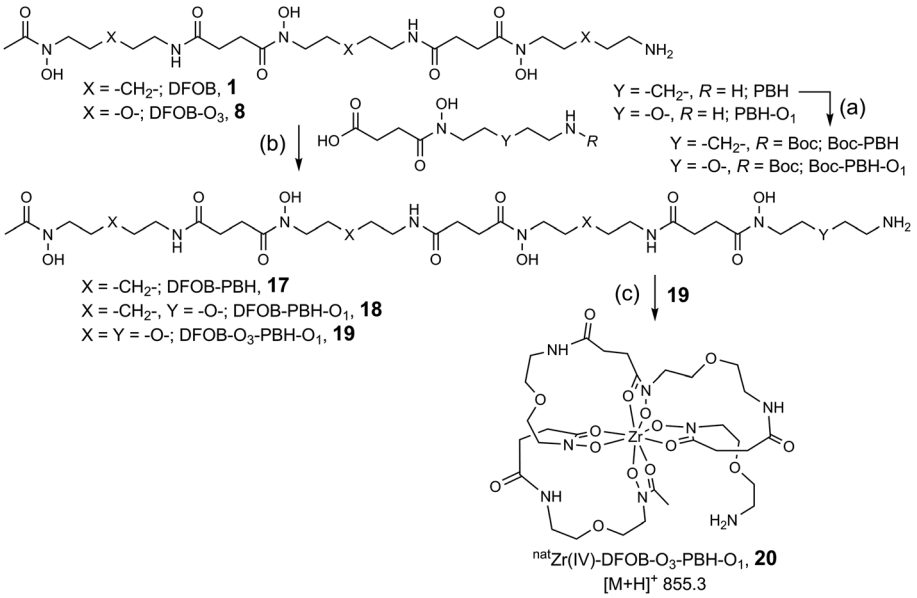

Fig. 7 Chain-extension reaction between hexadentate DFOB (**1**) or an ether-containing analogue (**8**) and *endo*-hydroxamic acid monomers (PBH, PBH-O_1) to furnish octadentate ligands (**17–19**) with variable water solubility. Reaction between ^{nat}Zr(IV) and **19** formed **20**. Reagents and conditions: (a) Boc_2O, $NaHCO_3$, 1 : 1 TFA/H_2O; (b) (i) DSC, Et_3N, DMF, (ii) 10% TFA/DCM; (c) ^{nat}Zr(acac)$_4$, 1 : 5 MeOH : H_2O, 15 min.

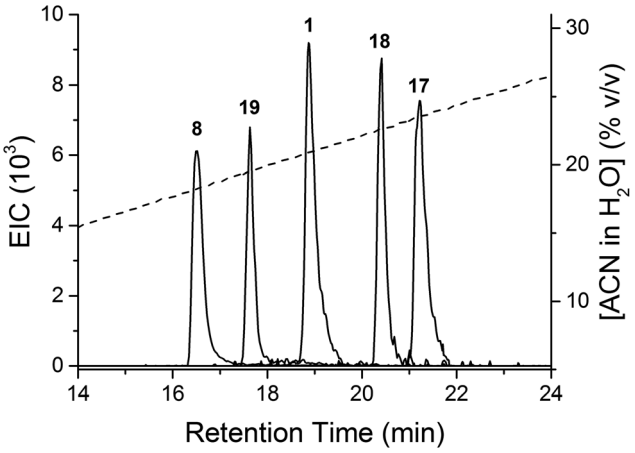

Fig. 8 LC-MS profiles of **1**, **8**, **17–19** trace acquired under the same gradient conditions, with respective EIC scaling factors of 0.5, 0.025, 0.2, 0.4, 1.

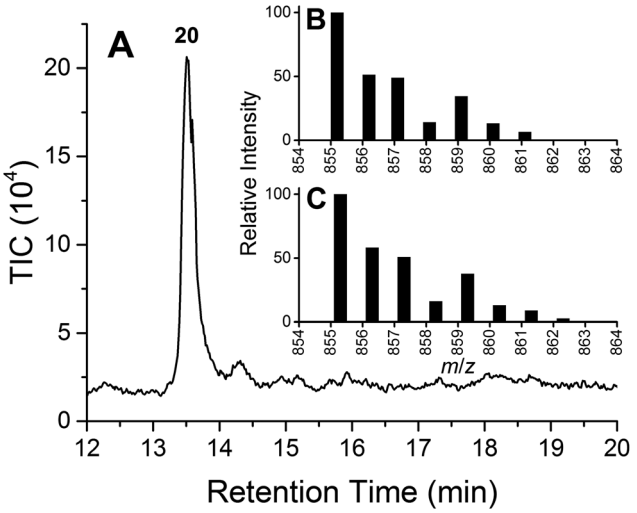

Fig. 9 LC trace using TIC detection from **20** (**A**), with MS isotope patterns shown in insets as experimental (**B**) or calculated (**C**).

H_2O : methanol) and **19** in water analysed after a 15 min incubation period at room temperature showed a single signal at t_R = 13.50 min (Fig. 9A), which gave an experimental MS isotope pattern (Fig. 9B) that agreed with the calculated pattern (Fig. 9C) for ^{nat}Zr(IV)–DFOB-O_3–PBH-O_1 (**20**). The identity of **20** was verified using HRMS, with characteristic isotope patterns observed for $[M + H]^+$, $[M + Na]^+$ and $[M + H + Na]^{2+}$ adducts (Table S3, Fig. S15–S17†). The ability to conduct the complexation reaction in an aqueous solution at neutral pH exemplifies the improved solubility properties of **19**, compared to the methylene analogue **17**. The earlier retention time of **20** (t_R = 16.52 min) compared to **19** (t_R = 17.63 min), as observed in an experiment conducted under different gradient conditions, showed ^{nat}Zr(IV) complexation did not negatively affect water solubility.

Conclusion

Analogues of DFOB containing one, two or three oxygen atoms in the main-chain region of the molecule were produced in OBEA-supplemented cultures of *S. pilosus*. The best-resolved adducts DFOB-O_1[001] (**2**), DFOB-O_2[110] (**6**) and DFOB-O_3[111] (**8**) were significantly more water soluble than DFOB (**1**), with

Published on 20 June 2017. Downloaded by University of Sydney on 2/26/2024 10:29:47 PM.

the maximum increase of 45 times measured for **8**, compared to **1**. This marked increase in water solubility resulting from the methylene-for-ether isostere exchange was engineered with only a minimal increase in molecular weight. This could be an advantage compared to a more conventional PEGylation approach, which could incur a significant increase in the molecular weight of DFOB, which already has a relatively high molecular weight. The chain-extension reaction between DFOB-O_3[111] (**8**) and an *endo*-hydroxamic acid amino carboxylic acid monomer that contained an ether oxygen atom in the main-chain region (PBH-O_1) produced DFOB-O_3–PBH-O_1 (**19**) as an octadentate chelate for Zr(IV) with improved water solubility than the methylene isostere DFOB–PBH. This work highlights the value of a combined microbiological-chemical approach to re-engineer natural products to meet clinical needs. The work identifies DFOB-O_3–PBH-O_1 (**19**) as a ligand with potential for development for immunological Zr-89 PET imaging.

Experimental procedures (materials and methods)

Culturing *S. pilosus*

S. pilosus (ATCC 19797) cultures were grown according to the protocol used in prior literature.[26] Selected cultures (50 mL) were supplemented with a solution of OBEA (10 mM in MilliQ water, pH 6.00 ± 0.05) after sterile filtering. Cultures were grown for 8 days (28 °C, 160 rpm), with siderophore production monitored by adding supernatant samples (200 μL) to a ferric assay solution (100 μL) containing ferric perchlorate (10 mM) in perchloric acid (200 mM). Absorbance at 500 nm was then measured using a BMG Labtech FLUOstar Omega microplate reader. Once siderophore production had plateaued, the supernatant was collected by centrifugation (4800 rpm, 20 min) for purification.

Purification of supernatant

Amberlite® XAD-2 resin (100 mL) was activated with stirring in methanol (300 mL, 15 min) in a 1 L glass beaker and removed by filtration. The resin was returned to the beaker and washed twice with water (300 mL, 15 min). The *S. pilosus* supernatant (50 mL) was diluted to 300 mL in MilliQ water and mixed in a batch extraction mode with XAD-2 resin (60 min) to adsorb siderophores amongst other low-molecular-weight organic compounds. The suspension was filtered and the filtrate retained as the first fraction. The siderophore-loaded XAD-2 resin was washed with water (300 mL, 15 min) to remove unbound components, with the filtrate retained as the second fraction. The siderophore-loaded XAD-2 resin was then washed with aqueous methanol (50% v/v, 300 mL, 15 min) to elute bound compounds, with the filtrate retained as the third fraction. This step was repeated four times to give fractions four through seven. The fractions were analysed for siderophores by the CAS assay.[48,53] The CAS positive fractions were pooled and taken to dryness *in vacuo* using a Buchi Rotavapor R-300. The subsequent purification using Ni(II)-IMAC and the desalting steps were consistent with previous methodology.[26]

LC-MS-Q analysis and LC purification

The XAD-2 and IMAC purified supernatant was analysed by LC-MS using an Agilent system, which consisted of a 1260 series quaternary pump with inbuilt degasser, a 1200 series autosampler, a temperature-controlled column compartment, a diode array detector, a fraction collector and a 6120 series single quadrupole mass spectrometer. The drying gas flow, temperature and nebuliser of the mass spectrometer were set to 12 L min^{-1}, 350 °C and 35 psi, respectively. Agilent OpenLAB chromatography data system ChemStation Edition (B.04.02) software was used for data acquisition and processing. An analytical Eclipse XDB-C18 reverse-phased prepacked column (particle size: 5 μm; 4.6 × 150 mm internal diameter) was used with a 0–30% ACN : H_2O (0.1% formic acid v/v) gradient over 40 min and a 0.2 mL min^{-1} flow rate. The injection volume was 35 μL and the capillary voltage of the ESI-MS was 4000 V. The resolution of more hydrophobic compounds was achieved with modified conditions (gradient of 0–50% ACN : H_2O (45 min at 0.5 mL min^{-1})). Semi-preparative LC was used to isolate individual peaks from the XAD-2 and IMAC purified supernatant. For this, a semi-preparative Eclipse XDB-C18 reverse-phased prepacked column (particle size: 5 μm; 9.4 × 250 mm internal diameter) was used with a 0–30% ACN : H_2O (0.1% formic acid v/v) gradient over 60 min, with a 1 mL min^{-1} flow rate and injection volume of 100 μL. Collected fractions were lyophilised using a Labconco FreeZone freeze-dryer.

LC-MS/MS-QQQ analysis

Individual peaks from the XAD-2 and Ni(II)-IMAC purified supernatant were analysed by LC-MS/MS-QQQ fragmentation using an Agilent system, which consisted of a 1290 series quaternary pump with inbuilt degasser, a 1200 series autosampler, a temperature-controlled column compartment, a diode array detector and a 6460 series triple quadrupole mass spectrometer with jet stream technology. Collision energy voltages were optimised for individual precursor ions and ranged from 16 to 28 V. The fragmentor voltage, drying gas flow, temperature and nebuliser of the mass spectrometer were set to 150 V, 10 mL min^{-1}, 300 °C and 25 psi, respectively. The column and LC conditions were identical to those used for LC-MS-Q analysis. Agilent MassHunter Workstation (B.07.01) software was used for data acquisition and processing.

Determination of log *P* values

Partition coefficients were determined by the shake-flask method using presaturated 1-octanol and MilliQ water. 1-Octanol (0.5 mL) was added to water (0.5 mL) containing dissolved DFOB, DFOB-O_1, DFOB-O_2, DFOB-O_3, DFOB–PBH, DFOB–PBH-O_1 or DFOB-O_3–PBH-O_1 in an Eppendorf tube (final concentration 2 mM for all compounds). The mixtures were shaken (250 rpm) on an orbital shaker for 20 hours and then aliquots of each phase (40 μL) were analysed by LC-MS on a 0–30% ACN : H_2O gradient over 40 min at a flow rate of

 This journal is © The Royal Society of Chemistry 2017

Published on 20 June 2017. Downloaded by University of Sydney on 2/26/2024 10:29:47 PM.

0.2 mL min^{-1}. The concentration of each compound was calculated for the aqueous and organic layers by peak area using extracted ion chromatograms.

NMR spectroscopy and HRMS

NMR (^{1}H, ^{13}C) spectroscopy was carried out using a Varian 400-MR NMR spectrometer (Lexington, MA) at a frequency of 399.73 (^{1}H) or 100.51 (^{13}C) MHz at 24 °C operated with VnmrJ 3.1 software (Agilent Technologies, Santa Clara, CA). The spectral data are reported in ppm (δ) relative to their residual solvent peaks ($CDCl_3$: δ_H 7.26, δ_C 77.23, CD_3OD: δ_H 3.31, δ_C 49.00, DMSO-d_6: δ_H 2.50, δ_C 39.52). The ^{13}C NMR spectrum for **8** (5000 scans) was obtained using a Shigemi tube (DMS-005TB, Shigemi Inc., Japan). Coupling constants (J) are reported in Hz and splitting patterns are reported as singlet (s), doublet (d), triplet (t), quartet (q) and quintet (qn). High-resolution mass spectra (HRMS, Table S2†) were recorded on a Bruker 7 T FT-ICR, in the School of Chemistry, University of Sydney.

Chemistry reagents

All reagents were obtained from Sigma-Aldrich, solvents were obtained from Univar. All chemicals were used as received. Reactions were monitored by ascending TLC using pre-coated plates (silica gel 60 F_{254}, 250 μm, Merck, Darmstadt, Germany), spots were visualised under ultraviolet light at both 254 nm and 365 nm and stained with basic potassium permanganate dip or $FeCl_3$ in ethanol. Davisil silica gel 60 Å, 60–100 mesh was used for silica gel chromatography.

2-(2-(2-Bromoethoxy)ethyl)isoindoline-1,3-dione (S1)

A suspension of phthalimide potassium salt (4.6 g, 19.9 mmol), 1,1′-oxybis[2-bromoethane] (5.54 g, 3.00 mL, 29.9 mmol) and $NaHCO_3$ (1.64 g, 19.9 mmol) in DMF (50 mL) was stirred for 6 h. The reaction mixture was diluted with ethyl acetate (150 mL) and washed with water (2 × 150 mL) and brine (150 mL). The organic layer was dried over Na_2SO_4, concentrated *in vacuo* and purified by silica gel chromatography eluting with 1 : 5 ethyl acetate/hexane to give an off white solid (yield: 4.08 g, 69%). ^{1}H NMR (400 MHz, $CDCl_3$): δ 7.78–7.84 (m, 2H), 7.65–7.70 (m, 2H), 3.87 (t, J = 7.2 Hz, 2H), 3.71–3.77 (m, 4H), 3.63 (t, J = 7.5 Hz, 2H); ^{13}C NMR (101 MHz, $CDCl_3$): δ 168.3, 156.8, 135.7, 134.1, 132.3, 129.6, 128.6, 128.5, 123.4, 81.5, 77.1, 67.7, 67.3, 49.8, 37.5, 28.4.

tert-Butyl benzyloxy(2-(2-(1,3-dioxoisoindolin-2-yl)ethoxy)ethyl) carbamate (S2)

Sodium hydride 60% dispersion in mineral oil (0.55 g, 13.7 mmol) was added portion-wise to a stirring solution of *tert*-butyl *N*-(benzyloxy)carbamate (2.05 g, 9.18 mmol) in DMF (15 mL) under a nitrogen atmosphere at ambient temperature. The reaction mixture was stirred for 15 min. **S1** (3.00 g, 10.1 mmol) in DMF (10 mL) was added dropwise and the reaction mixture was stirred under a nitrogen atmosphere at ambient temperature overnight. The reaction mixture was quenched with water (100 mL) and extracted with ethyl acetate (3 × 100 mL). The organic layers were pooled, washed with brine (100 mL), dried over Na_2SO_4 and concentrated *in vacuo*. The residue was purified by silica gel chromatography eluting with 1 : 4 ethyl acetate/hexane to give a yellow oil (yield: 1.94 g, 37%). ^{1}H NMR (400 MHz, $CDCl_3$): δ 7.78–7.82 (m, 2H), 7.65–7.70 (m, 2H), 7.29–7.37 (m, 5H), 4.77 (s, 2H), 3.87 (t, J = 7.2 Hz, 2H), 3.69 (t, J = 7.2 Hz, 2H), 3.60–3.62 (m, 2H), 3.54–3.57 (m, 2H), 1.45 (s, 9H); ^{13}C NMR (101 MHz, $CDCl_3$): δ 168.3, 156.8, 135.8, 134.1, 132.3, 129.6, 128.6, 128.5, 123.4, 81.5, 77.1, 67.7, 67.3, 49.8, 37.5, 28.4.

tert-Butyl benzyloxy(2-(2-(((benzyloxy)carbonyl)amino)ethoxy) ethyl)carbamate (S3)

S2 (1.5 g, 3.33 mmol), 50% aqueous hydrazine hydrate (0.53 g, 0.98 mL, 16.6 mmol) in ethanol (100 mL) was stirred under reflux for 3 h. The precipitate was filtered and washed with ethyl acetate (100 mL). The filtrate was concentrated *in vacuo* and dissolved in 1 : 1 1,4-dioxane/H_2O (50 mL). The mixture was cooled with an ice-water bath and $NaHCO_3$ (0.41 g, 5.00 mmol) and benzylchloroformate (0.85 g, 0.71 mL, 5.00 mmol) were added. The reaction mixture was allowed to warm to ambient temperature and stirred overnight. The reaction mixture was extracted with ethyl acetate (3 × 100 mL) and the organic layer was washed with water (100 mL) and brine (100 mL). The organic layer was dried over Na_2SO_4, concentrated *in vacuo* and the residue was purified by silica gel chromatography eluting with 1 : 4 ethyl acetate/hexane to give a clear gum (yield: 458 mg, 31%). ^{1}H NMR (400 MHz, $CDCl_3$): δ 7.27–7.39 (m, 10H), 5.31–5.40 (m, 1H), 5.09 (s, 2H), 4.82 (s, 2H), 3.56–3.61 (m, 4H), 3.51 (t, J = 6.9 Hz, 2H), 3.36 (dt, J = 6.9, 6.9 Hz, 2H), 1.48 (s, 9H). ^{13}C NMR (101 MHz, $CDCl_3$): δ 157.3, 156.7, 136.9, 135.8, 129.6, 128.8, 128.7, 128.6, 128.6, 128.3, 128.2, 81.8, 70.0, 67.3, 66.8, 49.4, 41.1, 28.5.

10-(Benzyloxy)-3,11-dioxo-1-phenyl-2,7-dioxa-4,10-diazatetradecan-14-oic acid (S4)

S3 (400 mg, 0.90 mmol) was dissolved in 10% TFA/dichloromethane (5 mL) and stirred for 2 h. The reaction mixture was concentrated *in vacuo* and dissolved in pyridine (5 mL). Succinic anhydride (109 mg, 1.08 mmol) was add and the reaction mixture was stirred at 90 °C for 2 h under a nitrogen atmosphere. The reaction mixture was cool to ambient temperature and stirred overnight under a nitrogen atmosphere. The reaction mixture was concentrated *in vacuo* and purified by silica gel chromatography eluting with 1 : 4 : 95 AcOH/MeOH/DCM to give a yellow gum (yield: 192 mg, 40%). ^{1}H NMR (400 MHz, CD_3OD): δ 7.25–7.44 (m, 10H), 5.01 (s, 2H), 4.92 (s, 2H), 3.74–3.88 (m, 2H), 3.60–3.74 (m, 2H), 3.48 (t, J = 7.2 Hz, 2H), 3.26 (t, J = 7.2 Hz, 2H), 2.69–2.75 (m, 2H), 2.48–2.58 (m, 2H). ^{13}C NMR (101 MHz, CD_3OD): δ 176.1, 158.8, 138.3, 136.2, 130.6, 129.9, 129.7, 129.4, 128.9, 128.8, 77.5, 70.6, 67.8, 67.4, 58.3, 47.1, 41.7, 28.6, 18.4.

4-((2-(2-Aminoethoxy)ethyl)(hydroxy)amino)-4-oxobutanoic acid (S5) (PBH-O_1)

A solution of **S4** (100 mg, 0.23 mmol) and 10% Pd/C (30 mg) in methanol (5 mL) was purged with N_2 gas, evacuated under

Published on 20 June 2017. Downloaded by University of Sydney on 2/26/2024 10:29:47 PM.

vacuum and purged with H_2 gas. The reaction mixture was stirred under a H_2 atmosphere overnight. Water (1 mL) was added to the reaction mixture and 10% Pd/C was carefully removed through a sintered funnel and washed with 1 : 1 methanol/water mixture (5 mL). The filtrate was concentrated *in vacuo* to give white solid (yield 49 mg, quantitative). ^{1}H NMR (400 MHz, CD_3OD): δ 3.81 (t, J = 4.8 Hz, 2H), 3.71 (t, J = 4.8 Hz, 2H), 3.65–3.67 (m, 2H), 3.04–3.12 (m, 2H), 2.71 (t, J = 6.8 Hz, 2H), 2.55 (t, J = 6.8 Hz, 2H); ^{13}C NMR (101 MHz, CD_3OD): δ 179.96, 175.93, 67.88, 67.55, 48.41, 40.63, 31.13, 29.06. HRMS (ESI-TOF) m/z: $[M + H]^+$ calcd for $C_8H_{16}N_2O_5$: 221.11320; found: 221.11329.

11-Hydroxy-2,2-dimethyl-4,12-dioxo-3,8-dioxa-5,11-diazapentadecan-15-oic acid (S6)

A solution of Boc_2O (38 mg, 0.18 mmol), **S5** (35 mg, 0.16 mmol) and $NaHCO_3$ (26 mg, 0.32 mmol) in 1 : 1 THF/H_2O (1 mL) was stirred for 6 h. The reaction mixture was diluted with ethyl acetate (25 mL) and washed with 0.5 M aqueous citric acid (25 mL). The organic layer was concentrated and purified by silica gel chromatography 1 : 20 MeOH/DCM to give a clear gum (yield: 21 mg, 41%). ^{1}H NMR (400 MHz, CD_3OD): δ 3.78 (t, J = 5.6 Hz, 2H), 3.65 (t, J = 5.6 Hz, 2H), 3.48 (t, J = 5.6 Hz, 2H), 3.20 (t, J = 5.2 Hz, 2H), 2.78 (t, J = 5.2 Hz, 2H), 2.57 (t, J = 5.6 Hz, 2H).

N^1-(1-Amino-6,17-dihydroxy-7,10,18,21-tetraoxo-3-oxa-6,11,17,22-tetraazaheptacosan-27-yl)-N^1-hydroxy-N^4-(5-(*N*-hydroxyacetamido)pentyl)succinamide; DFOB–PBH-O_1 (18)

A solution of **S6** (21 mg, 0.06 mmol), *N*,*N*′-disuccinimidyl carbonate (18 mg, 0.07 mmol) and Et_3N (18 μL, 13 mg, 0.12 mmol) in anhydrous DMF (1 mL) was stirred under a nitrogen atmosphere for 4 h. DFOB mesylate (7 mg, 0.01 mmol) in DMF (1 mL) was added and the reaction mixture stirred overnight. The reaction mixture was concentrated *in vacuo*, re-dissolved in 1 : 9 TFA/DCM (1 mL) and stirred for 2 h. The reaction mixture was concentrated *in vacuo* and re-dissolved in 1 : 1 DMSO/H_2O and purified by semi-preparative HPLC to give a white powder (yield: 1 mg, 12% from DFOB). ^{1}H NMR (400 MHz, DMSO-d_6): δ 7.74–7.81 (m, 2H), 2.97–3.02 (m, 6H), 2.57 (t, J = 6.0 Hz, 4H), 2.26 (t, J = 7.2 Hz, 4H), 1.32–1.54 (m, 12H), 1.16–1.29 (m, 6H). HRMS (ESI-TOF) m/z: $[M + H]^+$ calcd for $C_{33}H_{62}N_8O_{12}$: 763.45600; found: 763.45612.

N^1-(27-Amino-11,22-dihydroxy-7,10,18,21-tetraoxo-3,14,25-trioxa-6,11,17,22-tetraazaheptacosyl)-N^1-hydroxy-N^4-(2-(2-(*N*-hydroxyacetamido)ethoxy)ethyl)succinamide; DFOB-O_3–PBH-O_1 (19)

A solution of **S6** (21 mg, 0.06 mmol), *N*,*N*′-disuccinimidyl carbonate (18 mg, 0.07 mmol) and Et_3N (18 μL, 13 mg, 0.12 mmol) in anhydrous DMF (1 mL) was stirred under a nitrogen atmosphere for 4 h. The compound DFOB-O_3 (**8**) (7 mg, 0.01 mmol) in DMF (1 mL) was added and the reaction mixture stirred overnight. The reaction mixture was concentrated *in vacuo*, re-dissolved in 1 : 9 TFA/DCM (1 mL) and stirred for 2 h. The reaction mixture was concentrated *in vacuo* and re-dissolved in 1 : 1 DMSO/H_2O and purified by semi-preparative HPLC to give a white powder (yield: 2 mg, 21% from DFOB-O_3 (**8**)). ^{1}H NMR (400 MHz, DMSO-d_6): δ 8.39 (s, 2H), 7.80–7.90 (m, 3H), 3.64 (t, J = 5.2 Hz, 6H), 3.52–3.57 (m 8H), 3.47 (t, J = 5.2 Hz, 2H), 3.39 (t, J = 5.2 Hz, 8H), 3.16 (q, J = 5.2 Hz, 6H), 2.78 (t, J = 4.9 Hz, 2H), 2.60 (t, J = 7.2 Hz, 6H), 2.98 (t, J = 7.2 Hz, 6H), 1.98 (s 3H); HRMS (ESI-TOF) m/z: $[M + H]^+$ calcd for $C_{30}H_{56}N_8O_{15}$: 769.39379; found: 769.39434.

Abbreviations

DFOB	Desferrioxamine B
DP	1,5-Diaminopentane
EIC	Extracted ion chromatograms
LC-MS	Liquid chromatography-mass spectrometry
OBEA	Oxybis(ethanamine)
SIM	Selected ion monitoring
TIC	Total ion current.

Acknowledgements

This work was supported by the Australian Research Council (DP140100092) and the Australian Commonwealth Government (Australian Postgraduate Awards to T. R.-S. and T. J. T.). The University of Sydney is also acknowledged for support (CDIP 04-2015). A/Prof A. Katsifis is acknowledged for useful discussions.

References

1 E. W. Price and C. Orvig, Matching chelators to radiometals for radiopharmaceuticals, *Chem. Soc. Rev.*, 2014, **43**, 260–290.
2 P. J. Blower, A nuclear chocolate box: the periodic table of nuclear medicine, *Dalton Trans.*, 2015, **44**, 4819–4844.
3 D. Brasse and A. Nonat, Radiometals: towards a new success story in nuclear imaging?, *Dalton Trans.*, 2015, **44**, 4845–4858.
4 T. W. Price, J. Greenman and G. J. Stasiuk, Current advances in ligand design for inorganic positron emission tomography tracers ^{68}Ga, ^{64}Cu, ^{89}Zr and ^{44}Sc, *Dalton Trans.*, 2016, **45**, 15702–15724.
5 M. A. Deri, B. M. Zeglis, L. C. Francesconi and J. S. Lewis, PET imaging with ^{89}Zr: From radiochemistry to the clinic, *Nucl. Med. Biol.*, 2013, **40**, 3–14.
6 M. J. W. D. Vosjan, L. R. Perk, G. W. M. Visser, M. Budde, P. Jurek, G. E. Kiefer and G. A. M. S. van Dongen, Conjugation and radiolabeling of monoclonal antibodies with zirconium-89 for PET imaging using the bifunctional chelate *p*-isothiocyanatobenzyl-desferrioxamine, *Nat. Protoc.*, 2010, **5**, 739–743.

 This journal is © The Royal Society of Chemistry 2017

Published on 20 June 2017. Downloaded by University of Sydney on 2/26/2024 10:29:47 PM.

7 R. K. Scharli, R. I. Price, S. Chan, D. Cryer, C. M. Jeffery, A. H. Asad, L. Morandeau, P. Eu, C. Cullinane, A. Kasbollah and A. Katsifis, Establishing reliable production of the PET isotope 89Zr for research use: From target fabrication to preclinical imaging, *AIP Conf. Proc.*, 2012, **1509**, 101–107.

8 B. D. Wright and S. E. Lapi, Designing the magic bullet? The advancement of immuno-PET into clinical use, *J. Nucl. Med.*, 2013, **54**, 1171–1174.

9 C. T. Mendler, T. Gehring, H.-J. Wester, M. Schwaiger and A. Skerra, ^{89}Zr-labeled versus ^{124}I-labeled αHER2 Fab with optimized plasma half-life for high-contrast tumor imaging in vivo, *J. Nucl. Med.*, 2015, **56**, 1112–1118.

10 W. Tieu, T. Lifa, A. Katsifis and R. Codd, Octadentate zirconium(IV)-loaded macrocycles with varied stoichiometry assembled from hydroxamic acid monomers using metal-templated synthesis, *Inorg. Chem.*, 2017, **56**, 3719–3728.

11 F. Guérard, M. Beyler, Y.-S. Lee, R. Tripier, J.-F. Gestin and M. W. Brechbiel, Investigation of the complexation of ^{nat}Zr(IV) and ^{89}Zr(IV) by hydroxypyridinones for the development of chelators for PET imaging applications, *Dalton Trans.*, 2017, **46**, 4749–4758.

12 D. N. Pandya, N. Bhatt, H. Yuan, C. S. Day, B. M. Ehrmann, M. Wright, U. Bierbach and T. J. Wadas, Zirconium tetraazamacrocycle complexes display extraordinary stability and provide a new strategy for zirconium-89-based radiopharmaceutical development, *Chem. Sci.*, 2017, **8**, 2309–2314.

13 W. E. Meijs, J. D. M. Herscheid, H. J. Haisma and H. M. Pinedo, Evaluation of desferal as a bifunctional chelating agent for labeling antibodies with Zr-89, *Appl. Radiat. Isot.*, 1992, **43**, 1443–1447.

14 J. P. Holland, V. Divilov, N. H. Bander, P. M. Smith-Jones, S. M. Larson and J. S. Lewis, ^{89}Zr-DFO-J591 for immunoPET of prostate-specific membrane antigen expression *in vivo*, *J. Nucl. Med.*, 2010, **51**, 1293–1300.

15 E. J. Keliher, J. Yoo, M. Nahrendorf, J. S. Lewis, B. Marinelli, A. Newton, M. J. Pittet and R. Weissleder, ^{89}Zr-Labeled dextran nanoparticles allow in vivo macrophage imaging, *Bioconjugate Chem.*, 2011, **22**, 2383–2389.

16 M. J. Evans, J. P. Holland, S. L. Rice, M. G. Doran, S. M. Cheal, C. Campos, S. D. Carlin, I. K. Mellinghoff, C. L. Sawyers and J. S. Lewis, Imaging tumor burden in the brain with ^{89}Zr-transferrin, *J. Nucl. Med.*, 2013, **54**, 90–95.

17 J. P. Holland, M. J. Evans, S. L. Rice, J. Wongvipat, C. L. Sawyers and J. S. Lewis, Annotating MYC status with ^{89}Zr-transferrin imaging, *Nat. Med.*, 2012, **18**, 1586–1591.

18 P. K. E. Börjesson, Y. W. S. Jauw, R. Boellaard, R. de Bree, E. F. I. Comans, J. C. Roos, J. A. Castelijns, M. J. W. D. Vosjan, J. A. Kummer, C. R. Leemans, A. A. Lammertsma and G. A. M. S. van Dongen, Performance of immuno-positron emission tomography with zirconium-89-labeled chimeric monoclonal antibody U36 in the detection of lymph node metastases in head and neck cancer patients, *Clin. Cancer Res.*, 2006, **12**, 2133–2140.

19 L. R. Perk, O. J. Visser, M. Stigter-van Walsum, M. J. Vosjan, G. W. Visser, J. M. Zijlstra, P. C. Huijgens and G. A. van Dongen, Preparation and evalulation of ^{89}Zr-Zevalin for monitoring of ^{90}Y-Zevalin biodistribution with positron emission tomography, *Eur. J. Nucl. Med. Mol. Imaging*, 2006, **33**, 1337–1345.

20 P. K. E. Börjesson, Y. W. S. Jauw, R. de Bree, J. C. Roos, J. A. Castelijns, C. R. Leemans, G. A. M. S. van Dongen and R. Boellaard, Radiation dosimetry of ^{89}Zr-labeled chimeric monoclonal antibody U36 as used for immuno-PET in head and neck cancer patients, *J. Nucl. Med.*, 2009, **50**, 1828–1836.

21 S. N. F. Rizvi, O. J. Visser, M. J. D. Vosjan, A. Lingen, O. S. Hoekstra, J. M. Zijlstra, P. C. Huijgens, G. A. M. S. Dongen and M. Lubberink, Biodistribution, radiation dosimetry and scouting of ^{90}Y-ibritumomab tiuxetan therapy in patients with relapsed B-cell non-Hodgkin's lymphoma using ^{89}Zr-ibritumomab tiuxetan and PET, *Eur. J. Nucl. Med. Mol. Imaging*, 2012, **39**, 512–520.

22 E. C. Dijkers, T. H. Oude Munnink, J. G. Kosterink, A. H. Brouwers, P. J. Jager, J. R. de Jong, G. A. van Dongen, C. P. Schroeder, M. N. Lub-de Hooge and E. G. de Vries, Biodistribution of ^{89}Zr-trastuzumab and PET imaging of HER2-positive lesions in patients with metastatic breast cancer, *Clin. Pharmacol. Ther.*, 2010, **87**, 586–592.

23 L. R. Perk, M. J. W. D. Vosjan, G. W. M. Visser, M. Budde, P. Jurek, G. E. Kiefer and G. A. M. S. van Dongen, *p*-Isothiocyanatobenzyl-desferrioxamine: A new bifunctional chelate for facile radiolabeling of monoclonal antibodies with zirconium-89 for immuno-PET imaging, *Eur. J. Nucl. Med. Mol. Imaging*, 2010, **37**, 250–259.

24 R. C. Hider and X. Kong, Chemistry and biology of siderophores, *Nat. Prod. Rep.*, 2010, **27**, 637–657.

25 N. Ejje, C. Z. Soe, J. Gu and R. Codd, The variable hydroxamic acid siderophore metabolome of the marine actinomycete *Salinispora tropica* CNB-440, *Metallomics*, 2013, **5**, 1519–1528.

26 T. J. Telfer, M. P. Gotsbacher, C. Z. Soe and R. Codd, Mixing up the pieces of the desferrioxamine B jigsaw defines the biosynthetic sequence catalyzed by DesD, *ACS Chem. Biol.*, 2016, **11**, 1452–1462.

27 F. Guérard, Y.-S. Lee, R. Tripier, L. P. Szajek, J. R. Deschamps and M. W. Brechbiel, Investigation of Zr(IV) and ^{89}Zr(IV) complexation with hydroxamates: progress towards designing a better chelator than desferrioxamine B for immuno-PET imaging, *Chem. Commun.*, 2013, **49**, 1002–1004.

28 J. P. Holland and N. Vasdev, Charting the mechanism and reactivity of zirconium oxalate with hydroxamate ligands using density functional theory: Implications in new chelate design, *Dalton Trans.*, 2014, **43**, 9872–9884.

29 L. R. Perk, G. W. M. Visser, M. J. W. D. Vosjan, M. Stigter-van Walsum, B. M. Tijink, C. R. Leemans and G. A. M. S. van Dongen, ^{89}Zr as a PET surrogate radioisotope for scouting biodistribution of the therapeutic radiometals ^{90}Y and ^{177}Lu in tumor-bearing nude mice after coupling to

Published on 20 June 2017. Downloaded by University of Sydney on 2/26/2024 10:29:47 PM.

the internalizing antibody cetuximab, *J. Nucl. Med.*, 2005, **46**, 1898–1906.
30 J. P. Holland, E. Caldas-Lopes, V. Divilov, V. A. Longo, T. Taldone, D. Zatorska, G. Chiosis and J. S. Lewis, Measuring the pharmacodynamic effects of a novel Hsp90 inhibitor on HER2/*neu* expression in mice using ^{89}Zr-DFO-trastuzumab, *PLoS One*, 2010, **5**, e8859.
31 D. S. Abou, T. Ku and P. M. Smith-Jones, *In vivo* biodistribution and accumulation of ^{89}Zr in mice, *Nucl. Med. Biol.*, 2011, **38**, 675–681.
32 A. J. Chang, R. DeSilva, S. Jain, K. Lears, B. Rogers and S. Lapi, ^{89}Zr-Radiolabeled trastuzumab imaging in orthotopic and metastatic breast tumors, *Pharmaceuticals*, 2012, **5**, 79–93.
33 M. A. Deri, S. Ponnala, B. M. Zeglis, G. Pohl, J. J. Dannenberg, J. S. Lewis and L. C. Francesconi, Alternative chelator for ^{89}Zr radiopharmaceuticals: radiolabeling and evaluation of 3,4,3,-(LI-1,2-HOPO), *J. Med. Chem.*, 2014, **57**, 4849–4860.
34 M. Patra, A. Bauman, C. Mari, C. A. Fischer, O. Blacque, D. Haussinger, G. Gasser and T. L. Mindt, An octadentate bifunctional chelating agent for the development of stable zirconium-89 based molecular imaging probes, *Chem. Commun.*, 2014, **50**, 11523–11525.
35 S. E. Rudd, P. Roselt, C. Cullinane, R. J. Hicks and P. S. Donnelly, A desferrioxmaine B squaramide ester for the incorporation of zirconium-89 into antibodies, *Chem. Commun.*, 2016, **52**, 11889–11892.
36 D. J. Vugts, C. Klaver, C. Sewing, A. J. Poot, K. Adamzek, S. Huegli, C. Mari, G. W. M. Visser, I. E. Valverde, G. Gasser, T. L. Mindt and G. A. M. S. van Dongen, Comparison of the octadentate bifunctional chelator DFO*-*p*Phe-NCS and the clinically used hexadentate bifunctional chelator DFO-*p*Phe-NCS for 89-Zr-immuno-PET, *Eur. J. Nucl. Med. Mol. Imaging*, 2017, **44**, 286–295.
37 J. Liu, D. Obando, L. G. Schipanski, L. K. Groebler, P. K. Witting, D. S. Kalinowski, D. R. Richardson and R. Codd, Conjugates of desferrioxamine B (DFOB) with derivatives of adamantane or with orally available chelators as potential agents for treating iron overload, *J. Med. Chem.*, 2010, **53**, 1370–1382.
38 J. M. Harris and R. B. Chess, Effect of PEGylation on pharmaceuticals, *Nat. Rev. Drug Discovery*, 2003, **2**, 214–221.
39 T.-L. Cheng, K.-H. Chuang, B.-M. Chen and S. R. Roffler, Analytical measurement of PEGylated molecules, *Bioconjugate Chem.*, 2012, **23**, 881–899.
40 J. Meiwes, H.-P. Fiedler, H. Zähner, S. Konetschny-Rapp and G. Jung, Production of desferrioxamine E and new analogues by directed fermentation and feeding fermentation, *Appl. Microbiol. Biotechnol.*, 1990, **32**, 505–510.
41 S. Konetschny-Rapp, G. Jung, K. N. Raymond, J. Meiwes and H. Zaehner, Solution thermodynamics of the ferric complexes of new desferrioxamine siderophores obtained by directed fermentation, *J. Am. Chem. Soc.*, 1992, **114**, 2224–2230.
42 R. Thiericke and J. Rohr, Biological variation of microbial metabolites by precursor-directed biosynthesis, *Nat. Prod. Rep.*, 1993, **10**, 265–289.
43 R. J. Bergeron and J. J. Pegram, An efficient total synthesis of desferrioxamine B, *J. Org. Chem.*, 1988, **53**, 3131–3134.
44 F. Barona-Gomez, U. Wong, A. E. Giannakopulos, P. J. Derrick and G. L. Challis, Identification of a cluster of genes that directs desferrioxamine biosynthesis in *Streptomyces coelicolor*, M145, *J. Am. Chem. Soc.*, 2004, **126**, 16282–16283.
45 N. Kadi, D. Oves-Costales, F. Barona-Gomez and G. L. Challis, A new family of ATP-dependent oligomerization-macrocyclization biocatalysts, *Nat. Chem. Biol.*, 2007, **3**, 652–656.
46 N. Braich and R. Codd, Immobilized metal affinity chromatography for the capture of hydroxamate-containing siderophores and other Fe(III)-binding metabolites from bacterial culture supernatants, *Analyst*, 2008, **133**, 877–880.
47 R. Codd, J. Gu, N. Ejje and T. Lifa, New Applications of Immobilized Metal Ion Affinity Chromatography in Chemical Biology, in *Inorganic Chemical Biology: Principles, Techniques and Applications*, ed. G. Gasser, John Wiley & Sons, Ltd, Chichester, UK, 2014, pp. 1–35.
48 C. Z. Soe and R. Codd, Unsaturated macrocyclic dihydroxamic acid siderophores produced by *Shewanella putrefaciens* using precursor-directed biosynthesis, *ACS Chem. Biol.*, 2014, **9**, 945–956.
49 W. Keller-Schierlein, P. Mertens, V. Prelog and A. Wasler, Metabolic products of microorganisms. XLIX. Ferrioxamines A_1, A_2, and D_2, *Helv. Chim. Acta*, 1965, **48**, 710–723.
50 B. Borgias, A. D. Hugi and K. N. Raymond, Isomerization and solution structures of desferrioxamine B complexes of aluminum(3+) and gallium(3+), *Inorg. Chem.*, 1989, **28**, 3538–3545.
51 M. A. Boggs, H. Mason, Y. Arai, B. A. Powell, A. B. Kersting and M. Zavarin, Nuclear magnetic resonance spectroscopy of aqueous plutonium(IV) desferrioxamine B complexes, *Eur. J. Inorg. Chem.*, 2014, 3312–3321.
52 P. M. Ihnat, J. L. Vennerstrom and D. H. Robinson, Synthesis and solution properties of deferoxamine amides, *J. Pharm. Sci.*, 2000, **89**, 1525–1536.
53 B. Schwyn and J. B. Neilands, Universal chemical assay for the detection and determination of siderophores, *Anal. Biochem.*, 1987, **160**, 47–56.

 This journal is © The Royal Society of Chemistry 2017